Götz, J., Lueth, S., Henninges, J., Reinsch, T. (2018): Vertical seismic profiling using a daisy-chained deployment of fibre-optic cables in four wells simultaneously - Case study at the Ketzin carbon dioxide storage site. - *Geophysical Prospecting*, *66*, 6, pp. 1201—1214.

DOI: http://doi.org/10.1111/1365-2478.12638

Title page

Title:

Vertical Seismic Profiling using a daisy-chained deployment of fibre optic cables in four wells simultaneously – Case study at the Ketzin CO_2 storage site

Authors: Julia Götz[1], Stefan Lüth[2*], Jan Henninges[2], Thomas Reinsch[2]

1: BAW Federal Waterways Engineering and Research Institute, Karlsruhe, Germany (formerly at GFZ).

2: GFZ German Research Centre for Geosciences, Potsdam, Germany.

*: Corresponding author, Tel.: +49(0)3312881558, Email: slueth@gfz-potsdam.de.

Abstract: The geological storage of carbon dioxide (CO_2) is considered as one of the measures to reduce greenhouse gas emissions and to mitigate global warming. Operators of storage sites are required to demonstrate safe containment and stable behaviour of the storage complex which is achieved by geophysical and geochemical monitoring, combined with reservoir simulations. For site characterization, as well as for imaging the CO_2 plume in the reservoir complex and detecting potential leakage, surface and surface-borehole time-lapse seismic monitoring surveys are the most wide-spread and established tools. At the Ketzin pilot site for CO_2 storage, permanently installed fibre optic cables, initially deployed for Distributed Temperature Sensing (DTS), were used as seismic receiver arrays, demonstrating their ability to provide high-resolution images of the storage formation. A VSP experiment was acquired using 23 source point locations and the daisy-chained deployment of a fibre optic cable in four wells as a receiver array. The data were used to generate a 3D VSP cube, complementing the large scale 3D surface seismic measurements by a high resolution image of the reservoir close to the injection well. Stacking long vibro-sweeps at each source location, resulted in VSP shot gathers characterized by a signal-to-noise ratio similar to gathers acquired using geophones. A detailed data analysis shows strong dependency of data quality on borehole conditions with significantly better signal-to-noise ratio in regions with good coupling conditions.

Keywords: Acquisition, Borehole geophysics, Monitoring.

References

Barberan, C., Allanic, C., Avila, D., Hy-Billiot, J., Hartog, A., Frignet, B. and Lees, G. (2012). Multi-offset Seismic Acquisition Using Optical Fiber Behind Tubing. 74th EAGE Conference & Exhibition incorporating SPE EUROPEC 2012, Copenhagen, Denmark, extended abstract Y003.

Baumann, G., Henninges, J. and De Lucia, M. (2014). Monitoring of saturation changes and salt precipitation during CO_2 injection using pulsed neutron-gamma logging at the Ketzin site. Intl J Greenhouse Gas Control 28, 134-146.

Bergmann, P., Ivandic, M., Norden, B., Rücker, C., Kiessling, D., Lüth, S., Schmidt-Hattenberger, C. and Juhlin, C. (2014). Case History: Combination of seismic reflection and constrained resistivity inversion with an application to 4D imaging of the CO_2 storage site, Ketzin, Germany. Geophysics 79(2), B37–B50.

Chadwick, A., Williams, G., Delepine, N., Clochard, V., Labat, K., Sturton, S., Buddensiek, M.-L., Dillen, M., Nickel, M., Lima, A. L., Arts, R., Neele, F. and Rossi, G. (2010). Quantitative analysis of time-lapse seismic monitoring data at the Sleipner CO_2 storage operation. The Leading Edge 29(2), 170–177.

Cosma, C. and Enescu, N. (2001). Characterization of fractured rock in the vicinity of tunnels by the swept impact seismic technique. International Journal of Rock Mechanics & Mining Sciences 38, 815–821.

Daley, T., Freifeld, B., Ajo-Franklin, J., Dou, S., Pevzner, R., Shulakova, V., Kashikar, S., Miller, D., Götz, J., Henninges, J. and Lüth, S. (2013). Field testing of fiber-optic distributed acoustic sensing (DAS) for subsurface seismic monitoring. The Leading Edge 32, 699–706.

Daley, T.M., Miller, D.E., Dodds, K., Cook, P. & Freifeld, B.M. 2016. Field testing of modular borehole monitoring with simultaneous distributed acoustic sensing and geophone vertical seismic profiles at Citronelle, Alabama. Geophysical Prospecting 64, 1318–1334.

Dean, T., Cuny, T. & Hartog, A.H. 2017. The effect of gauge length on axially incident P-waves measured using fibre optic distributed vibration sensing. Geophysical Prospecting 65, 184–193.

Dillon, P.B. and Thomson, R.C. (1984). Offset source VSP surveys and their image reconstruction. Geophysical Prospecting 32, 790–811.

Egreteau, A., Gibson, J., Lin F. and Meunier, J. (2009). Using long sweep in land vibroseis acquisition. 71st EAGE Conference & Exhibition, Amsterdam, The Netherlands, extended abstract.

Förster A., Norden B., Zinck-Jørgensen K., Frykman P., Kulenkampff J., Spangenberg E., Erzinger J., Zimmer M., Kopp J., Borm G., Juhlin C., Cosma C. and Hurter S. (2006). Baseline characterization of the CO_2SINK geological storage site at Ketzin, Germany. Environmental Geosciences 13(3), 145–161.

Förster, A., Schöner, R., Förster, H.-J., Norden, B., Blaschke, A.-W., Luckert, J., Beutler, G., Gaupp, R. and Rhede, D. (2010). Reservoir characterization of a CO_2 storage aquifer: The Upper Triassic Stuttgart Formation in the Northeast German Basin. Marine and Petroleum Geology 27, 2156–2172.

Frignet, B. and Hartog, A. (2014). Optical Vertical Seismic Profile On Wireline Cable. SPWLA 55th Annual Logging Symposium, Abu Dhabi, May 18-22, extended abstract.

Giese, R., Henninges, J., Lüth, S., Morozova, D., Schmidt-Hattenberger, C., Würdemann, H., Zimmer, M., Cosma, C. and Juhlin, C. (2009). Monitoring at the CO_2SINK site: A concept integrating geophysics, geochemistry and microbiology. Energy Procedia, 1(1), 2251–2259.

Götz, J. (2014). Borehole seismic monitoring of CO_2 storage within a saline aquifer at Ketzin, Germany. PhD Thesis, TU Berlin, Germany, 125 p.

Götz, J., Lüth, S., Krawczyk, C.M., and Cosma, C. (2014). Zero-Offset VSP Monitoring of CO_2 Storage: Impedance Inversion and Wedge Modelling at the Ketzin Pilot Site. International Journal of Geophysics, 2014, Article ID 294717, 15 pages.

Götz, J., Lüth, S., Henninges, J. and Reinsch T. (2015). Using a fibre optic cable as Distributed Acoustic Sensor for Vertical Seismic Profiling at the Ketzin CO_2 storage site. - 77th EAGE Conference & Exhibition, Madrid, Spain, extended abstract Th P2 13.

Hansen, O., Eiken, O., Ostmo, S., Johansen, R.I., and Smith, A. (2011). Monitoring CO_2 injection into a fluvial brine-filled sandstone formation at the Snøhvit field, Barents Sea. SEG San Antonio 2011 Annual Meeting, extended abstract SEG-2011-4092.

Hardage, B.A. 2000. Vertical seismic profiling: principles; Third updated and revised edition. Pergamon, ISBN 0-08-043518-1.

Hartog, A., Kotov, O., and Liokumovich, L. (2013). The Optics of Distributed Vibration Sensing. - Second EAGE Workshop on Permanent Reservoir Monitoring 2013 - Current and Future Trends Stavanger, Norway, extended abstract Th_01_04.

Hartog, A., Frignet, B., Mackie, D. and Clark, M. (2014). Vertical seismic optical profiling on wireline logging cable. Geophysical Prospecting, 62(4), 693–701.

95 Henninges, J., Liebscher, A., Bannach, A., Brandt, W., Hurter, S., Köhler, S., Möller, F. and CO_2SINK-
96 Group (2011). P-T-ρ and two-phase fluid conditions with inverted density profile in observation wells
97 at the CO_2 storage site at Ketzin (Germany). Energy Procedia 4, 6085–6090.

98 Hill, D. (2013). Distributed Acoustic Sensing for Permanent Downhole Monitoring. Second EAGE
99 Workshop on Permanent Reservoir Monitoring 2013 - Current and Future Trends Stavanger, Norway,
100 extended abstract Th_01_05.

101 Hovorka, S.D., Benson, S.M., Doughty, C., Freifeld, B.M., Sakurai, S., Daley, T.M., Kharaka, Y.K., Holtz,
102 M.H., Trautz, R.C., Nance, H.S., Myer, L.R. and Knauss, K.G. (2006). Measuring permanence of CO_2
103 storage in saline formations: the Frio experiment. Environmental Geosciences 13(2), 105–121.

104 Hovorka, S.D., Meckel, T.A. and Treviño, R. H. (2013). Monitoring a large-volume injection at
105 Cranfield, Mississippi-Project design and recommendations. International Journal of Greenhouse Gas
106 Control 18, 345–360.

107 Huang, F., Juhlin, C., Kempka, T., Norden, B. and Zhang, F. (2015). Modeling 3D time-lapse seismic
108 response induced by CO_2 by integrating borehole and 3D seismic data - A case study at the Ketzin
109 pilot site, Germany. International Journal of Greenhouse Gas Control 36, 66–77.

110 Humphries, M., Vidal, J.A.M. and de Dios, J.C. (2015. VSP Monitoring for CO_2 Migration Tracking in
111 Fractured Rock Massifs. 77th EAGE Conference & Exhibition, Madrid, Spain, extended abstract Tu
112 N112 02.

113 IPCC (2005). Special Report on Carbon Dioxide Capture and Storage. Prepared by Working Group III of
114 the Intergovernmental Panel on Climate Change, Cambridge University Press, New York, NY, USA.

115 Ivandic, M., Yang, C., Lüth, S., Cosma, C. and Juhlin, C. (2012). Time-lapse analysis of sparse 3D
116 seismic data from the CO_2 storage pilot site at Ketzin, Germany. Journal of Applied Geophysics 84,
117 14–28.

118 Ivandic, M., Juhlin, C., Lüth, S., Bergmann, P., Kashubin, A., Sopher, D., Ivanova, A., Baumann, G. and
119 Henninges, J. (2015). Geophysical monitoring at the Ketzin pilot site for CO_2 storage: New insights
120 into the plume evolution. International Journal of Greenhouse Gas Control 32, 90–105.

121 Ivanova, A., Kashubin, A., Juhojuntti, N., Kummerow, J., Henninges, J., Juhlin, C., Lüth, S. and Ivandic,
122 M. (2012). Monitoring and volumetric estimation of injected CO_2 using 4D seismic, petrophysical
123 data, core measurements and well logging: a case study at Ketzin, Germany. Geophysical
124 Prospecting, 60(5), 957–973.

Juhlin, C., Giese, R., Zinck-Jørgensen, K., Cosma, C., Kazemeini, H., Juhojuntti, N., Lüth, S., Norden, B. and Förster, A. (2007). Case History: 3D baseline seismics at Ketzin, Germany: The CO_2SINK project. Geophysics, 72(5), B121–B132.

Kikuta, K., Hongo, S., Tanase, D. and Ohsumi, T. (2005). Field test of CO_2 injection in Nagaoka, Japan. In Proc. 7th Int. Conf. on Greenhouse Gas Control Technologies, vol. 2 (eds E.S. Rubin, D.W. Keith and C.F. Gilboy), 1367–1372. Oxford, UK: Elsevier.

Kuvshinov, B. N. (2015). Interaction of helically wound fibre-optic cables with plane seismic waves. Geophysical Prospecting, 64(3), 671-688.

Lüth, S., Ivanova, A., Ivandic, M. and Götz, J. (2015). 4D seismic monitoring at the Ketzin pilot site during five years of storage – results and quantitative assessment. Energy Procedia 76, 536–542.

Madsen, K., Thompson, M., Parker, T. and Finfer, D. (2013). A VSP field trial using distributed acoustic sensing in a producing well in the North Sea. First break 31, 51–56.

Martens, S., Liebscher, A., Möller, F., Henninges, J., Kempka, T., Lüth, S., Norden, B., Prevedel, B., Szizybalski, A., Zimmer, M., Kühn, M. and the Ketzin Group (2013). CO_2 storage at the Ketzin pilot site, Germany: Fourth year of injection, monitoring, modelling and verification. Energy Procedia 37, 6434–6443.

Martens, S., Möller, F., Streibel, M., Liebscher A. and The Ketzin Group (2014). Completion of five years of safe CO_2 injection and transition to the post-closure phase at the Ketzin pilot site. Energy Procedia 59, 190–197.

Martens, S., Conze, R., De Lucia, M., Henninges, J., Kempka, T., Liebscher, A., Lüth, L., Möller, F., Norden, B., Prevedel, B., Schmidt-Hattenberger, C., Szizybalski, Vieth-Hillebrand, A., Würdemann, H., Zemke, K. and Zimmer, M. (2015). Joint Research Project CO_2MAN (CO_2MAN Reservoir Management): Continuation of Research and Development Work for CO_2 Storage at the Ketzin Pilot Site. In: A. Liebscher and U. Münch (eds.), Geological Storage of CO_2 – Long Term Security Aspects, Advanced Technologies in Earth Sciences, Springer International Publishing Switzerland, 1–32.

Mateeva, A., Lopez, J., Potters, H., Mestayer, J., Cox, B., Kiyashchenko, D., Wills, P., Grandi, S., Hornman, K., Kuvshinov, B., Berlang, W., Yang, Z. and Detomo, R. (2014). Distributed acoustic sensing for reservoir monitoring with vertical seismic profiling. Geophysical Prospecting 62, 679–692.

Mateeva, A. and Zwartjes, P.M. (2017). Depth Calibration of DAS VSP Channels - A New Data-Driven Method. 79th EAGE Conference and Exhibition, extended abstract, DOI: 10.3997/2214-4609.201701201.

156 Mestayer, J., Cox, B., Wills, P., Kiyashchenko, D., Lopez, J., Costello, M., Bourne, S., Ugueto, G.,
157 Lupton, R., Solano, G., Hill, D. and Lewis, A. (2011). Field Trials of Distributed Acoustic Sensing for
158 Geophysical Monitoring. SEG Annual Meeting San Antonio, extended abstract.

159 Mewhort, L., Bezdan, S. and Jones, M. (2002). Does it Matter What Kind of Vibroseis Deconvolution is
160 Used? CSEG Geophysics, extended abstract, 1-4.

161 Molenaar, M., Hill, D., Webster, P., Fidan, E. and Birch, B. (2011). First Downhole Application of
162 Distributed Acoustic Sensing (DAS) for Hydraulic Fracturing Monitoring and Diagnostics. SPE
163 Hydraulic Fracturing Technology Conference, The Woodlands, Texas, extended abstract SPE 140561.

164 Norden, B. and Frykman, P. (2013). Geological modelling of the Triassic Stuttgart Formation at the
165 Ketzin CO_2 storage site, Germany. International Journal of Greenhouse Gas Control 19, 756–774.

166 Parker, T., Shatalin, S. and Farhadiroushan, M. (2014). Distributed Acoustic Sensing - a new tool for
167 seismic applications. First Break 32, 61–69.

168 Prevedel, B., Wohlgemuth, L., Legarth, B., Henninges, J., Schütt, H., Schmidt-Hattenberger, C.,
169 Norden, B., Förster, A. and Hurter, S. (2009). The CO_2SINK boreholes for geological CO_2-storage
170 testing. Energy Procedia 1, 2087–2094.

171 Prevedel, B., Martens, S., Norden, B., Henninges, J. and Freifeld, B.M. (2014). Drilling and
172 abandonment preparation of CO_2 storage wells – Experience from the Ketzin pilot site. Energy
173 Procedia 63, 6067–6078.

174 Reinsch, T., Henninges, J., Götz, J., Jousset, P., Bruhn, D. and Lüth, S. (2015). Distributed Acoustic
175 Sensing Technology for Seismic Exploration in Magmatic Geothermal Areas. Proceedings World
176 Geothermal Congress 2015, Melbourne, Australia, extended abstract.

177 Ringrose, P.S., Mathieson, A.S., Wright, I.W., Selama, F., Hansen, O., Bissell, R., Saoula, N. and
178 Midgley, J. (2013). The in Salah CO_2 storage project: lessons learned and knowledge transfer. Energy
179 Procedia 37, 6226–6236.

180 Schmidt-Hattenberger, C., Bergmann, P., Labitzke, T. and Wagner, F. (2014). CO_2 migration
181 monitoring by means of Electrical Resistivity Tomography (ERT) - Review on five years of operation of
182 a permanent ERT system at the Ketzin pilot site. Energy Procedia 6, 4366–4373.

183 Staples, R.K., Hobbs, R.W. and White, R.S. (1999). A comparison between airguns and explosives as
184 wide-angle seismic sources. Geophysical Prospecting 47, 313–339.

185 Underschultz, J., Boreham, C., Dance T., Stalker, L., Freifeld, B., Kirste, D. and Ennis-King, J. (2011).
186 CO_2 storage in a depleted gas field: an overview of the CO2CRC Otway Project and initial results.
187 International Journal of Greenhouse Gas Control 5(4), 922–932.

188 Whittaker, S., Rostron, B., Hawkes C., Gardner, C., White, D., Johnson, J., Chalaturnyk, R. and
189 Seeburger, D. (2011). A decade of CO2 injection into depleting oil fields: monitoring and research
190 activities of the IEA GHG Weyburn-Midale CO_2 monitoring and storage project. Energy Procedia 4,
191 6069–6076.

192 Yang, C., Juhlin, C., Enescu, N., Cosma, C., and Lüth, S. (2010). Moving source profile data processing,
193 modelling and comparison with 3D surface seismic data at the CO_2SINK project site, Ketzin, Germany.
194 Near Surface Geophysics 8, 601–610.

195 Yordkayhun, S., Ivanova, A., Giese, R., Juhlin, C. and Cosma, C. (2009). Comparison of surface seismic
196 sources at the CO_2SINK site, Ketzin, Germany. Geophysical Prospecting 57, 125–139.

197 Zhang, F., Juhlin, C., Cosma, C., Tryggvason, A. and Pratt, R. (2012). Cross-well seismic waveform
198 tomography for monitoring CO_2 injection: a case study from the Ketzin Site, Germany. Geophysical
199 Journal International 189(1), 629–646.

200

Figure captions:

Figure 1: Left: Location of the Ketzin CO_2 storage site. Right: Slices through the depth converted 3D surface seismic cube, showing main reflectors of the anticlinal structure in Ketzin. The CO_2 distribution in the reservoir (Stuttgart Formation) is based on the normalized amplitude difference between the 3D surface seismic repeat 2012 and the baseline 2005 (Ivandic *et al.* 2015).

Figure 2: Schematic illustration of casing, cementation (grey colour) and installation of the daisy-chained fibre-optic cable in the annulus outside the 5-1/2" production casing (except for Ktzi203, which has a 3-1/2" casing). The DAS readout unit was connected to a single-mode fibre.

Figure 3: Areal view of the storage site with an overlay showing the approximate lateral distribution of CO_2 in the reservoir in 2012 (Ivandic *et al.* 2015, Götz *et al.* 2015). The loci of the reflection points are determined by 3D ray tracing (Chapter 3) and shown as black lines. The layers of the Ketzin anticline dip at about 15° in NNE-SSW direction (Förster *et al.* 2006), which is the reason why the locations of the reflections points are centred north (up-dip) of the wells within a ~100 m radius of the wells.

Figure 4: Top: True vertical depth of the channels. Bottom: Correlated and stacked data (exemplary source point 7, 31 sweeps). The 5900 channels are recorded along the daisy-chained fibre optical cable (Figure 2), comprising cable sections along the surface as well as downward and upward sections within the wells. The blue polygons illustrate the windows used for the signal-to-noise ratio calculation (Chapter 5).

Figure 5: Illustration of 3D depth migration with the software VSProwess. Based on a structural model (Bergmann *et al.* 2014, Huang *et al.* 2015) and a velocity model (lower left image), the loci of the reflection points are calculated by 3D ray tracing (right image). The top left image is a top view, showing the source points (blue dots), the wells (green dots) and the loci of the calculated reflection points. The blue layer marks the depth of the top of the Stuttgart Formation (the reservoir).

Figure 6: Completion of the wells Ktzi200 – Ktzi203 with corresponding zero-offset VSP wavefields. The cementation of the wells (grey colour) and the installation of the fibre optical cable (red lines) are shown.

Figure 7: Evolution of the signal-to-noise ratios, when stacking the correlated data. Different vibrator drive levels are indicated by solid lines (high drive) and dashed-dotted lines (low drive). On the right hand side of the upper and lower row, the measured improvement of the signal-to-noise ratio is compared to the theoretical improvement with $\sqrt{n}$.

Figure 8: Comparison of zero-offset VSP data (exemplarily for Ktzi203 and shot point 6) for 1 sweep (left), a stack of 5 sweeps (middle) and a stack of 29 sweeps (right).

Figure 9: Comparison between the vertical component of borehole geophones (velocity, VIBSIST source) and the DAS recordings (strain rate, Vibroseis source). Left: Well completion of well Ktzi202 with the locations of 3C geophones (black dots) and the fibre-optical cable (red line). The optical fibre is installed behind the production casing. Cemented intervals are indicated by grey sections in the well diagram. Middle: Wiggle plot of the seismic traces. Right: Comparison of amplitude spectrum and signal-to-noise ratios for the depth interval 450 m – 700 m. Modified after Reinsch *et al.* 2015.

Figure 10: Comparison of bandpass filtered DAS-VSP cube (10-20-80-100 Hz) and the depth converted 3D surface seismic cube (Ivandic *et al.* 2015). For reasons of good visibility, the DAS-VSP slices are shown 12 m in front of the 3D surface seismic cube.

Figure 11: Comparison of 3D surface seismic, bandpass filtered DAS-VSP and raw DAS-VSP. Left: Top view on the seismic amplitudes extracted from the top of the Stuttgart Formation for the 3D seismic and DAS-VSP. The black shaded areas indicate the DAS-VSP reflection loci. Red line shows location of sections (right). Right: Cross sections extracted between the wells Ktzi201 and Ktzi202. The wells Ktzi201, Ktzi203 and Ktzi202 are indicated by the black lines and the impedance log for the well Ktzi201 is inserted (blue line).

Vertical Seismic Profiling using a daisy-chained deployment of fibre optic cables in four wells simultaneously – Case study at the Ketzin CO_2 storage site

Julia Götz[1], Stefan Lüth[2*], Jan Henninges[2], Thomas Reinsch[2]

1: BAW Federal Waterways Engineering and Research Institute, Karlsruhe, Germany (formerly at GFZ).

2: GFZ German Research Centre for Geosciences, Potsdam, Germany.

*: Corresponding Author, Tel.: +49(0)3312881558, Email: slueth@gfz-potsdam.de.

Abstract: The geological storage of carbon dioxide (CO_2) is considered as one of the measures to reduce greenhouse gas emissions and to mitigate global warming. Operators of storage sites are required to demonstrate safe containment and stable behaviour of the storage complex which is achieved by geophysical and geochemical monitoring, combined with reservoir simulations. For site characterization, as well as for imaging the CO_2 plume in the reservoir complex and detecting potential leakage, surface and surface-borehole time-lapse seismic monitoring surveys are the most wide-spread and established tools. At the Ketzin pilot site for CO_2 storage, permanently installed fibre optic cables, initially deployed for Distributed Temperature Sensing (DTS), were used as seismic receiver arrays, demonstrating their ability to provide high-resolution images of the storage formation. A VSP experiment was acquired using 23 source point locations and the daisy-chained deployment of a fibre optic cable in four wells as a receiver array. The data were used to generate a 3D VSP cube, complementing the large scale 3D surface seismic measurements by a high resolution image of the reservoir close to the injection well. Stacking long vibro-sweeps at each source location, resulted in VSP shot gathers characterized by a signal-to-noise ratio similar to gathers acquired using geophones. A detailed data analysis shows strong dependency of data quality on borehole conditions with significantly better signal-to-noise ratio in regions with good coupling conditions.

Keywords: Acquisition, Borehole geophysics, Monitoring.

1 Introduction

CCS, the capture and geological storage of carbon dioxide (CO_2), is discussed as one of several methods to reduce CO_2 emissions to the atmosphere and thus to keep global warning below the 2°C level (IPCC 2005). For increasing general acceptance of long-term storage of CO_2 in geological formations, and for advancing in storage operation and monitoring technologies, several sites for

geological CO_2 storage, from pilot scale to industrial scale, have been studied during the past decades. Among these sites are, for example, Frio and Cranfield (USA, e.g. Hovorka *et al.* 2006, Hovorka, Meckel and Treviño 2013), In Salah (Algeria, e.g. Ringrose *et al.* 2013), Ketzin (Germany, e.g. Martens *et al.* 2013), Nagaoka, (Japan, e.g. Kikuta *et al.* 2005), Otway (Australia, e.g. Underschultz *et al.* 2011), Sleipner and Snøhvit (Norway, e.g. Chadwick *et al.* 2010, Hansen *et al.* 2011) and Weyburn (Canada, e.g. Whittaker *et al.* 2011). Seismic measurements are crucial components of the characterization and monitoring programmes at these sites. Apart from conventional 2D and 3D surface seismic acquisition, particularly for the long-term monitoring of a CO_2 storage complex, permanently installed solutions are considered a useful contribution. Buried geophone and hydrophone arrays, but also fibre optic cables have been deployed at selected sites.

The Ketzin pilot site, located about 25 km west of Berlin, is the first on-shore geological CO_2 storage site in Europe. Within 5 years of injection (June 2008 – August 2013), 67 ktons of CO_2 were injected into a saline sandstone aquifer at 630 – 650 m depth below ground level (upper part of the Triassic Stuttgart Formation, Figure 1). Since August 2013, the site has been in the post-injection phase with continued monitoring activities. The site was abandoned by the end of 2017.

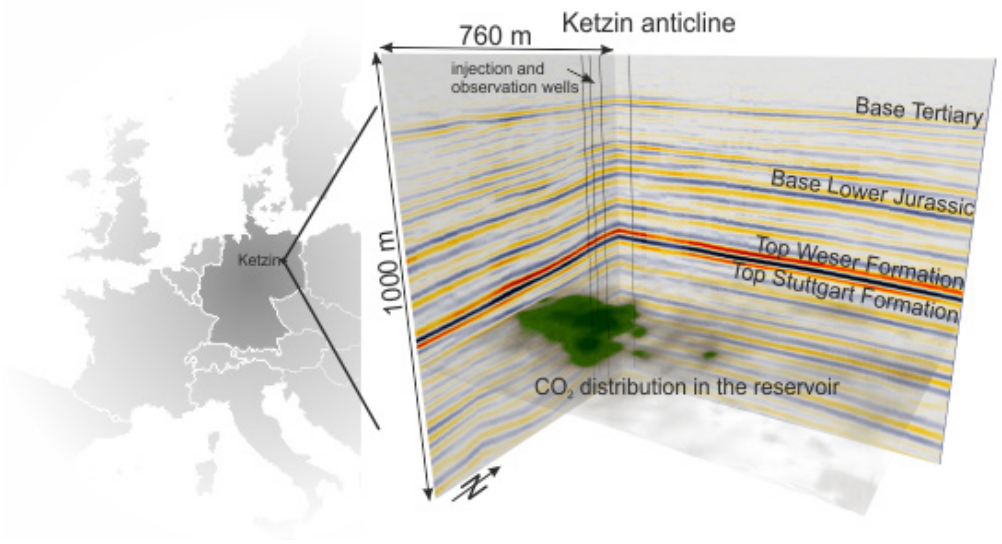

Figure 12: Left: Location of the Ketzin CO_2 storage site. Right: Slices through the depth converted 3D surface seismic cube, showing main reflectors of the anticlinal structure in Ketzin. The CO_2 distribution in the reservoir (Stuttgart Formation) is based on the normalized amplitude difference between the 3D surface seismic repeat 2012 and the baseline 2005 (Ivandic *et al.* 2015).

A comprehensive baseline characterization and monitoring program has been carried out since 2004, covering all life cycle phases of the storage site from development, injection to post closure (Giese *et al.* 2009, Martens *et al.* 2014, Martens *et al.* 2015). Borehole and surface geophysical monitoring comprises Electrical Resistivity Tomography (ERT), pulsed neutron-gamma logging, and seismic measurements, providing time-lapse images of the CO_2 distribution in the reservoir (Figure 1), as well

as saturation and mass estimations (e.g. Baumann, Henninges and De Lucia 2014, Bergmann *et al.* 2014, Schmidt-Hattenberger *et al.* 2014, Ivandic *et al.* 2015, Lüth *et al.* 2015).

Surface seismic monitoring comprises a baseline survey in 2005 followed by three repeats in 2009 (22 ktons of CO_2 injected, Ivanova *et al.* 2012), 2012 (Figure 1, 61 ktons of CO_2 injected, Ivandic *et al.* 2015), and 2015 (two years after injection closure). Besides the 3D seismic, 2D (pseudo 3D) seismic (Ivandic *et al.* 2012), Moving Source Profiling (MSP, downhole acquisition of dense shot profiles on the surface using sparse downhole receivers, Yang *et al.* 2010), offset and zero-offset VSP (Götz 2014, Götz *et al.* 2014) and crosshole seismic surveys (Zhang *et al.* 2012) were acquired.

The CO_2 distribution in the reservoir, based on the normalized amplitude difference between the 3D surface seismic repeat in 2012 and the baseline 2005 is shown in Figure 1. The Stuttgart formation originates from fluvial processes, for which reason the reservoir is lithologically heterogeneous (Förster *et al.* 2006). Horizontally and vertically heterogeneous permeability caused an irregular pattern of the CO_2 plume and its westward propagation, contrary to the expected propagation towards the top of the anticline in the northern direction.

As part of the monitoring program, the injection well and three observation wells at the Ketzin site were completed with various permanently installed downhole sensors for the continuous borehole monitoring of CO_2 injection (Prevedel *et al.* 2009). Four wells reaching through the reservoir were equipped with fibre-optic cables in the annulus outside the production casing. Along the optical fibres, continuous temperature measurements were performed using the Distributed Temperature Sensing (DTS) technique, based on optical Raman scattering (Henninges *et al.* 2011). Not only temperature, but also strain influences the signal of the backscattered light. When using an optical fibre as distributed acoustic sensor, the strain on the fibre, induced by the seismic wavefield or other acoustic disturbances, is recorded with high spatial and temporal resolution. In the literature, the technology is referred to as Distributed Acoustic Sensing (DAS) or Distributed Vibration Sensing (DVS) (e.g., Hartog, Kotov and Liokumovich 2013). A simpler version of this technique is used for detecting strain from non-seismic sources, such as, e.g., for continuous monitoring of pipelines, roads or borders and, increasingly during the last decade, for production monitoring from within the wellbore (Molenaar *et al.* 2011, Hill 2013).

Recording seismic data using DAS instead of geophones has advantages especially for borehole seismic measurements like Vertical Seismic Profiling (VSP). In wells with pre-existing optical cables (e.g. for Distributed Temperature Sensing, DTS), on-demand or time-lapse DAS-VSPs can be acquired without well intervention (Mateeva *et al.* 2014). The fibre optical cable covers the entire well at once; unlike in geophone recordings, it is not necessary to move the tool string and repeat the shot

(Mateeva *et al.* 2014). Fibre presence makes it feasible to interrogate several wells at the same time, with full vertical coverage. It is also possible to retrofit wells with fibre optical cables by deploying them along tubing, pumping them inside a control line (Mateeva *et al.* 2014) or to use wireline cables (Frignet and Hartog 2014, Hartog *et al.* 2014). Some points have to be taken into account when recording DAS-VSP data. The signal-to-noise ratio of DAS data is lower than that of geophones with current interrogator units. This can be overcome by investing in more source effort and in the future by improvements in cable design and interrogator units (Mateeva *et al.* 2014). With an optical fibre, one component representing the strain between two points within the fibre is measured. Therefore, the angular dependence is stronger than that of a 3C geophone (Kuvshinov, 2015). Due to uncertainties during the deployment of the fibre in a well, the DAS channels along the cable need to be assigned to an exact depth with respect to geology or well completion. Calibration points, such as the well head or well bottom can be used for this and are typically enough for short wells. For longer or more complicated wells, fibre distribution along the completion may not be uniform, necessitating additional calibration points or different calibration methods (e.g., Mateeva and Zwartjes, 2017).

Various DAS-VSP field tests have been published, especially CO_2 storage pilot sites provided the opportunity to test this new technology for geophysical reservoir monitoring, for example in Citronelle (Daley *et al.* 2013), Hontomin (Humphries, Vidal and de Dios 2015), Ketzin (Daley *et al.* 2013), Otway (Daley *et al.* 2013), Quest (Mestayer *et al.* 2011, Mateeva *et al.* 2014) and Rousse (Barberan *et al.* 2012). Along with publications from Frignet and Hartog (2014), Hartog *et al.* (2014), Madsen *et al.* (2013) or Parker, Shatalin and Farhadiroushan (2014) these case studies represent a wide range of different source types, source-receiver geometries and cable deployments (wireline, on tubing, behind casing).

This paper presents a successful DAS-VSP field test performed at the Ketzin pilot site for CO_2 storage. 23 VSP source points were recorded simultaneously in four wells and a depth migrated 3D DAS-VSP cube was built. The DAS-VSP cube complements the 3D surface seismic by providing a focused high resolution image of the reservoir complex below the injection site.

2 DAS-VSP experiment at the Ketzin site

At the Ketzin test site, four deep wells were drilled through the storage formation about 650 m depth to final depths between 690 m and 790 m (Figure 2, Figure 3 blue dots). The designation of the injection well (CO2 Ktzi201/2007) and the three observation wells (CO2 Ktzi200/2007, CO2 Ktzi202/2007, CO2 Ktzi203/2012) will be abbreviated with Ktzi200 – Ktzi203 hereafter. All wells

were equipped with fibre optic cables in the annulus outside the production casing used for Distributed Temperature Sensing (DTS) (Henninges *et al.* 2011). During the installation of the cables, custom-made casing centralizers were used to clamp the sensor cables to the casing and to protect them from mechanical damage during the installation (Prevedel *et al.* 2009). These casing centralizers were attached to every casing pipe at an interval of approximately 12.7 m. Only in deeper parts of the wells, the fibre-optical cable is cemented within the multiple casings system (Figure 2). For the DAS-VSP measurement the fibres were spliced together, resulting in a daisy-chained cable of 5900 m length, including parts on the surface, as well as downward and upward cable branches in the wells (Figure 2). This set-up allowed for acquisition at relatively low operational costs as only one interrogator was needed for acquisition in four wells. It should be noted that this set-up was deployed in relatively shallow wells, resulting in a total cable length which can be handled by one single interrogator still assuring a high optical sampling rate (10 kHz).

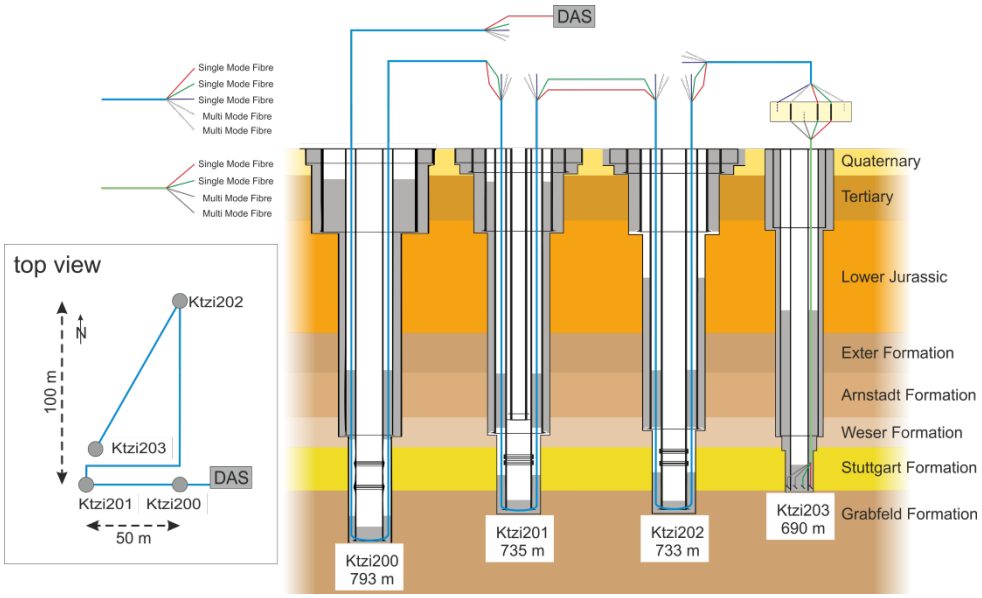

Figure 13: Schematic illustration of casing, cementation (grey colour) and installation of the daisy-chained fibre-optic cable in the annulus outside the 5-1/2" production casing (except for Ktzi203, which has a 3-1/2" casing). The DAS readout unit was connected to a single-mode fibre.

The described infrastructure was used for a first DAS-VSP field test in 2012, which proved that it was possible to record upgoing DAS-VSP reflections over the whole depth of the wells with an accelerated weight drop as seismic source (Daley *et al.* 2013). Based on the promising results an extended DAS-VSP campaign was conducted in May 2013. Seismic waves were generated at 23 source locations, distributed on the premises close to and in between the wells (Figure 3, red dots), allowing a high-resolution imaging of the reservoir right below the injection site (Götz *et al.* 2015). The signal was simultaneously recorded in four wells (Figure 3, blue dots) along the fibre-optic cable of 5900 m length with a DAS gauge length (distance over which strain rate is measured, e.g. Dean, Cuny and

Hartog 2017) of 10 m and a channel spacing of 1 m. The sampling frequency after the conversion into seismic data format was 1 kHz.

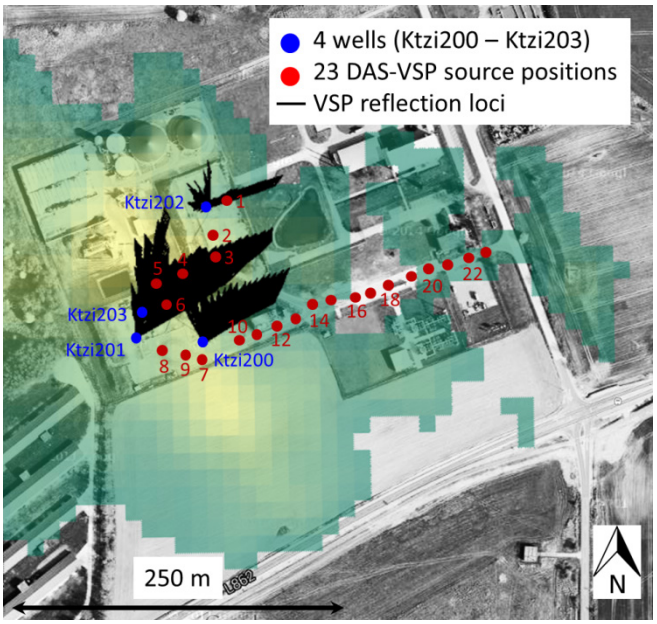

Figure 14: Areal view of the storage site with an overlay showing the approximate lateral distribution of CO_2 in the reservoir in 2012 (Ivandic *et al.* 2015, Götz *et al.* 2015). The loci of the reflection points are determined by 3D ray tracing (Chapter 3) and shown as black lines. The layers of the Ketzin anticline dip at about 15° in NNE-SSW direction (Förster *et al.* 2006), which is the reason why the locations of the reflections points are centred north (up-dip) of the wells within a ~100 m radius of the wells.

The locations of the source points were defined by the infrastructure, especially roads, on the premises of the storage site and were chosen in order to image the subsurface around and between the wells. The seismic vibrator "DMT Vibro-Truck Mertz M12" with a maximum peak force of 30,030 lbs (133.6 kN) was used as source. Considering the relatively small dimensions of the DAS-VSP experiment (about 800 m well depth, max. offset 260 m), this rather powerful seismic source was chosen to account for the expected reduced signal-to-noise ratio.

For the same reason, the data is vertically stacked, after recording 27 – 32 sweeps per source point. To maintain an acceptable productivity rate, a relatively long sweep length of 50 s (with 0.3 s taper) was chosen. The sweeps were excited as linear up-sweeps with frequencies from 7 – 120 Hz. The listening time was 5 s, the dead time of the DAS interrogator unit (time interval between the end of one recording and the beginning of the next one) was 5 s as well. Long sweeps of the length $n * L$ can be recorded faster than the equivalent of n sweeps of the length L, because the required listening time and dead time of the DAS readout unit has to be counted only once, instead of n times for the other case (Egreteau *et al.* 2009).

The time needed to record four wells (5900 channels, 5070 of them within the wells) with 27 – 32 sweeps, including the moving of the Vibroseis truck and the checking of the peak particle velocity

(PPV measurements) at structures which are sensitive to vibrations, was 45 minutes per source point on average.

In order to facilitate the assignment of true depth to DAS channels, several locations along the cable (especially close to the well heads) were calibrated by a tap test ("knocking onto the cable"). This is done by using recorded calibration points close to the well head and the location of the cable turnarounds within the wells. The depth of the cable turnaround was determined during installation relative to the position of the next casing joints. By comparing the depth calibrated VSP to the well completion (Chapter 4) and to geological markers like a 10 – 20 m thick anhydrite layer at the top of the Weser Formation (Figure 1) it is shown that a good assignment to true vertical depth is achieved.

The DAS interrogator was attached to a single mode fibre (Figure 2). After processing of the raw opto-electronic signal by Silixa Ltd., the seismic data was delivered as uncorrelated and unstacked SEGY files, in which the amplitudes are linearly related to the physical quantity "strain rate".

3 Processing and imaging

Processing consists of Vibroseis correlation with the pilot sweep, vertical stacking over repeated sweeps, the assignment of the DAS channels to the true vertical depth (Chapter 2), predictive deconvolution with the ~40 ms long downgoing wavelet for wavelet shaping followed by wavefield separation by median filtering.

Standard Vibroseis theory states the far-field particle displacement is proportional to the applied ground force, and the far-field particle velocity is proportional to the time derivative of the ground force (Mewhort, Bezdan and Jones 2002). As a result, when recording the particle velocity with geophones, the time derivative of the ground force is often used for the correlation. Since the DAS technology records the strain rate (not velocity as geophones), we tested different correlation approaches and observed that the same, nearly zero-phase, wavelet is produced for the following combinations: correlation of 1) the strain rate with the pilot sweep (ground force), 2) -1 times the strain rate with the ground force, 3) the strain (time integrated strain rate) and the time-derivative of the ground force. Finally, the pilot sweep was chosen for the correlation.

The data were correlated before stacking, thereby it was possible to check data quality and sort out disturbed records caused by e.g. the drive-by of heavy tractors on the premises (~3 % of the whole data set). After vertical stacking of the sweeps, the downward and upward cable branches (Figure 4) can be again vertically stacked, leading to about 60 stacks for the wells Ktzi200 to Ktzi202. Before stacking these cable branches, the cross-correlation of downgoing and upgoing trace pairs is calculated and the time-shift between the maximum of the cross-correlation and zero-lag is applied.

Generally, for all source locations the signal-to-noise ratio is high (Chapter 5) and direct P-waves as well as reflected P-waves can be identified (Figure 4).

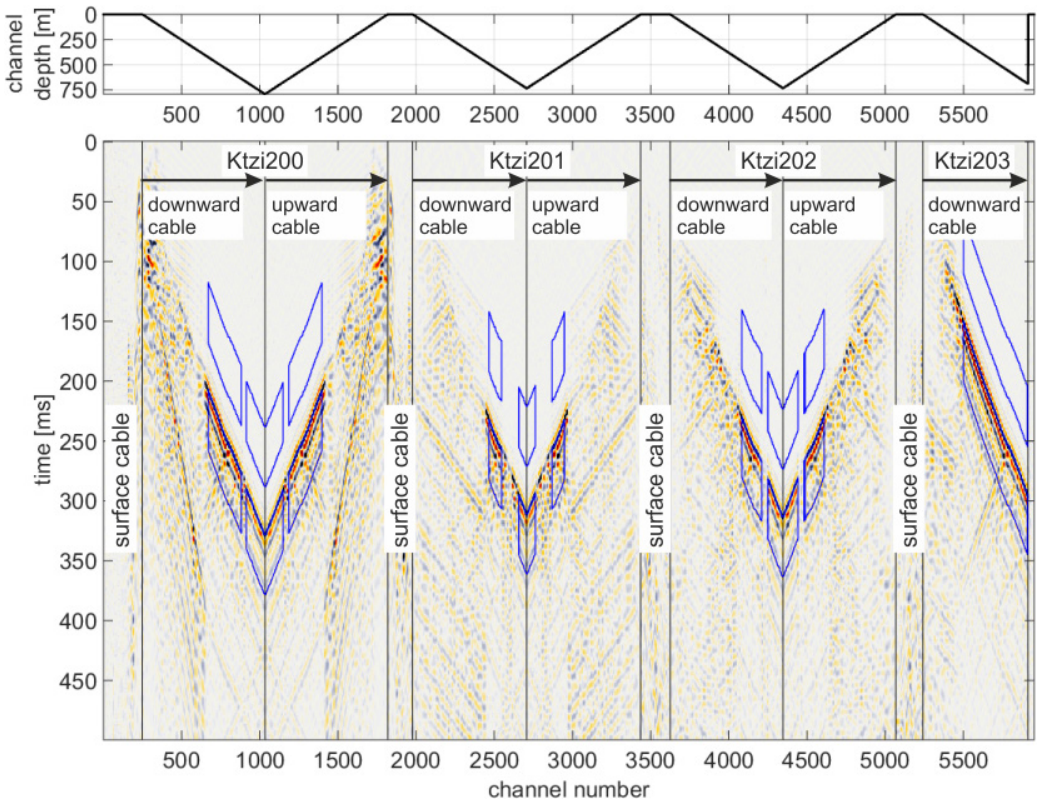

Figure 15: Top: True vertical depth of the channels. Bottom: Correlated and stacked data (exemplary source point 7, 31 sweeps). The 5900 channels are recorded along the daisy-chained fibre optical cable (Figure 2), comprising cable sections along the surface as well as downward and upward sections within the wells. The blue polygons illustrate the windows used for the signal-to-noise ratio calculation (Chapter 5).

The 3D depth migration of the reflected PP-wavefield was performed using the software VSProwess. The imaging is based on Dillon and Thomson (1984), but uses a 3D ray tracer to determine the location of the migration ellipses (Figure 5). A structural model is built based on the depth migrated 3D surface seismic and formation tops within the four Ketzin wells (Bergmann *et al.* 2014, Huang *et al.* 2015).

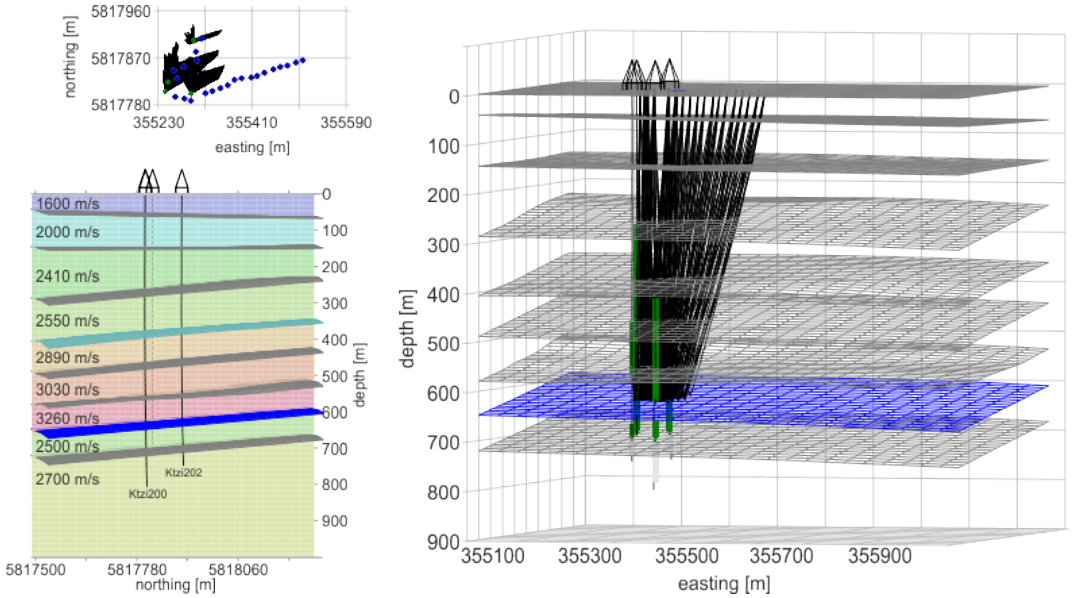

Figure 16: Illustration of 3D depth migration with the software VSProwess. Based on a structural model (Bergmann *et al.* 2014, Huang *et al.* 2015) and a velocity model (lower left image), the loci of the reflection points are calculated by 3D ray tracing (right image). The top left image is a top view, showing the source points (blue dots), the wells (green dots) and the loci of the calculated reflection points. The blue layer marks the depth of the top of the Stuttgart Formation (the reservoir).

The P-wave velocities are derived from sonic logs, and calibrated by comparing the picked and modelled first break travel times. The achieved root mean square error between the picked and modelled first break travel times is 4 ms (the sampling interval is 1 ms). Considering a mean P-wave velocity of 2600 m/s and the top of the Stuttgart Formation at 630 m depth (Figure 5, bottom left), an accuracy of $\pm$4 ms would lead to an uncertainty in the depth of this reflector of $\pm$10 m. The matching could be improved by using a heterogeneous velocity model, taking into account the variation of velocities within the layers.

4 Influence of casing on the DAS-VSP wavefield

The DAS-VSP data quality is affected by the partially cemented casings of the wells (Figure 6). It is well recognized that casing and cementing conditions have a strong influence on recorded VSP data (e.g. Hardage 2000). The most favorable situation is a well-cemented single casing string or an uncased open borehole. In contrast to this, multiple uncemented casing strings usually prevent usable VSP data from being recorded.

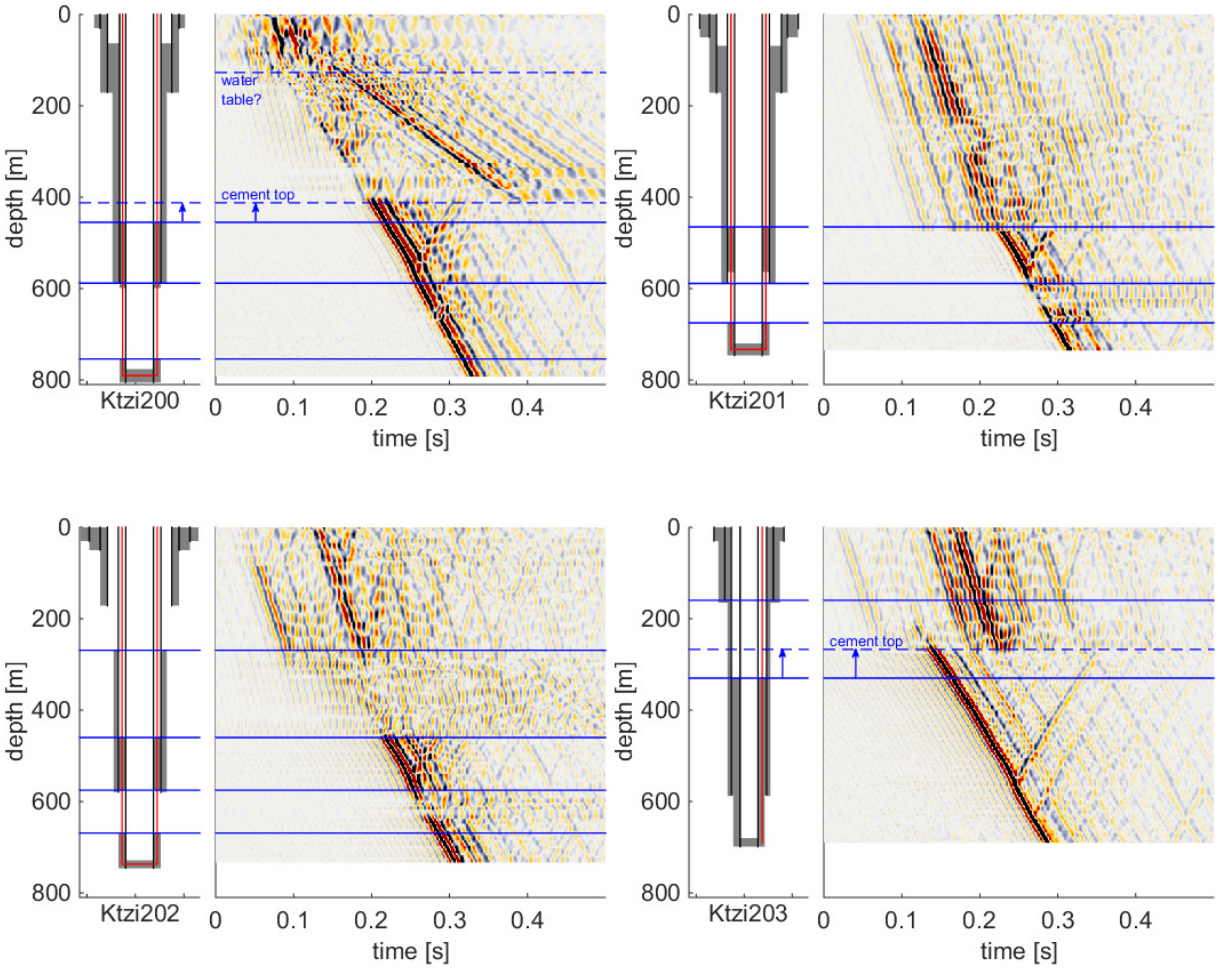

Figure 17: Completion of the wells Ktzi200 – Ktzi203 with corresponding zero-offset VSP wavefields. The cementation of the wells (grey colour) and the installation of the fibre optical cable (red lines) are shown.

In the upper sections of the wells, the DAS-VSP wavefield is dominated by casing waves and tube waves (multiple casing strings, partly uncemented). In the lower parts of the wells, where the casing strings are cemented to one another and also to the formation, the identification of direct P-waves is possible. The signal strength is reduced in depth ranges of uncemented and centralized single casing strings, but the identification of direct waves is still possible over most of these intervals. This general character of the recorded VSP data applies to all four wells, and has also been observed during previous VSP surveys recorded with conventional borehole geophones in the Ktzi202 well (Götz *et al.* 2014), which are described in more detail in Chapter 6 below. In case of the wells Ktzi200 and Ktzi203 (Figure 6, top left and bottom right), the DAS-VSP detects a higher cement top, than determined according to cement bond logs (Prevedel *et al.* 2014). This can be explained by continued hardening of the cement after measuring the cement bond logs. In Ktzi200 (Figure 6, top left), downgoing tube waves can be observed, possibly indicating the water table in the annulus of the casing. The main wave types which can be observed are casing waves, tube waves and downgoing as well as reflected P-waves. The influence of the casing is reduced for more distant source points in a way that the data

in uncemented sections is getting better. Due to cementation of Ktzi203 over a large depth range (Figure 6, bottom right), the best data quality is achieved for this well.

5 Signal-to-noise ratio: how many sweeps per source point?

The signal-to-noise ratio is calculated following the method described by Staples, Hobbs and White (1999) and Yordkayhun *et al.* (2009). For a given trace it is calculated by comparing the root mean squared (RMS) amplitude within a window above the first break (noise window) to the RMS amplitude within a window below the first break (signal window). This is described by

$$Q_{S/N} = \frac{S_{RMS}{}_{t_0}^{t_0+50\ ms}}{N_{RMS}{}_{t_0-40\ ms}^{t_0-90\ ms}}. \quad (1)$$

$Q_{S/N}$ is the signal-to-noise ratio; S_{RMS} and N_{RMS} describe the RMS amplitude calculated for signal and noise windows, respectively. The first break time is t_0. In the expression above, a 50 ms window for both noise and signal windows is defined. To carry out the calculation, the first breaks were picked automatically for traces not affected by casing waves. The signal window starts at the first break, whereas the noise window has an offset of 40 ms prior to the first breaks (Figure 4, blue polygons). The signal-to-noise value for the whole shot gather is calculated as the mean value over all considered traces in the four wells. The evolution of the signal-to-noise ratio, when stacking the correlated data, is shown in Figure 7.

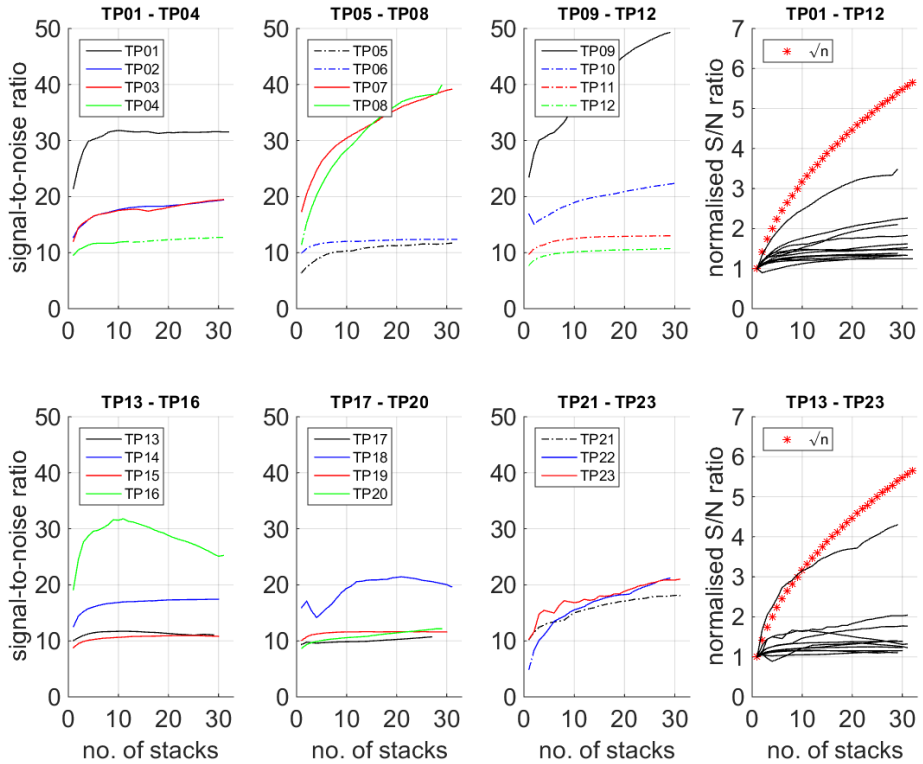

Figure 18: Evolution of the signal-to-noise ratios, when stacking the correlated data. Different vibrator drive levels are indicated by solid lines (high drive) and dashed-dotted lines (low

drive). On the right hand side of the upper and lower row, the measured improvement of the signal-to-noise ratio is compared to the theoretical improvement with $\sqrt{n}$.

In the vicinity of sensitive structures, like wells or CO_2 tanks, the force of the seismic vibrator was reduced from 80 % of the maximum peak force (high drive) to 40 % of the maximum peak force (low drive). Good signal-to-noise ratios of > 10, are achieved for all source points. In general, the signal-to-noise ratio is lower for the low drive level and it is reduced with the source offset.

In Figure 7 (right hand side of the upper and lower row) the measured improvement of the signal-to-noise ratio is compared to the theoretical improvement by the square-root of the number of stacks $\sqrt{n}$. The measured signal-to-noise ratios do not improve significantly while stacking sweeps, they remain well below $\sqrt{n}$, for some cases they even decline. This could be caused by coherent noise like correlation noise and the excitation of sweeps on instable concrete slabs, where it is hard to control the sweep leading to non-repeatable source signature. Considering the signal-to-noise ratio alone, recording of 5 sweeps per source point would have been sufficient. But this ratio, which is related to the first breaks, does not account for the dynamic of the seismic wavefield. Especially reflection amplitudes (upgoing P-waves) are improved by stacking all available sweeps (Figure 8). The phase of the wavelet in the first 5 sweeps is not zero-phase, probably due to systematic errors in the early sweeps. This could affect the signal-to-noise ratio for this shot gather and should be examined further.

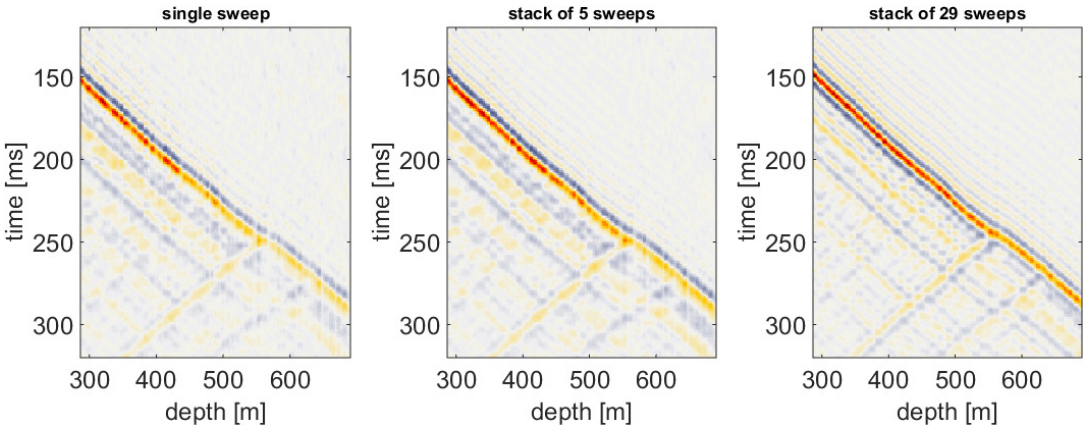

Figure 19: Comparison of zero-offset VSP data (exemplarily for Ktzi203 and shot point 6) for 1 sweep (left), a stack of 5 sweeps (middle) and a stack of 29 sweeps (right).

6 Zero-offset at the Ktzi202 well – DAS-VSP compared with geophone VSP

At the Ketzin CO_2 storage site, seismic downhole measurements were also performed with conventional three component borehole geophones (Daley *et al.* 2013, Götz *et al.* 2014). The zero-offset VSP was recorded with 3C-geophones lowered into the well and clamped inside the casing at

80 depth levels, from 325 m to 720 m below ground level (m b.gl.). The vertical distance between the geophones is 5 m. A stack of 32 sweeps from the zero-offset DAS-VSP in the Ktzi202 well is compared to data from a conventional zero-offset VSP recorded in the same well. The conventional zero-offset VSP was recorded in 2011, with a different type of seismic source, the VIBSIST, working according to the Swept Impact Seismic Technique (SIST, Cosma and Enescu 2001, Yang *et al.* 2010). The VIBSIST source uses an excavator-mounted hydraulic rock-breaker to produce a rapid series of impacts, maintaining a monotonic variation of the impact rate. The seismograms are obtained by cross-correlating the swept impact sequence with a pilot signal recorded at the source. Especially, the zero-offset VSP in Ketzin is affected by the only partially cemented production casing of the receiver well (Chapter 4), so the traces are compared for the lower part of the well, only. In Figure 9, the vertical components of the geophone recordings (physical quantity: velocity) are plotted together with the corresponding DAS traces (physical quantity: strain rate).

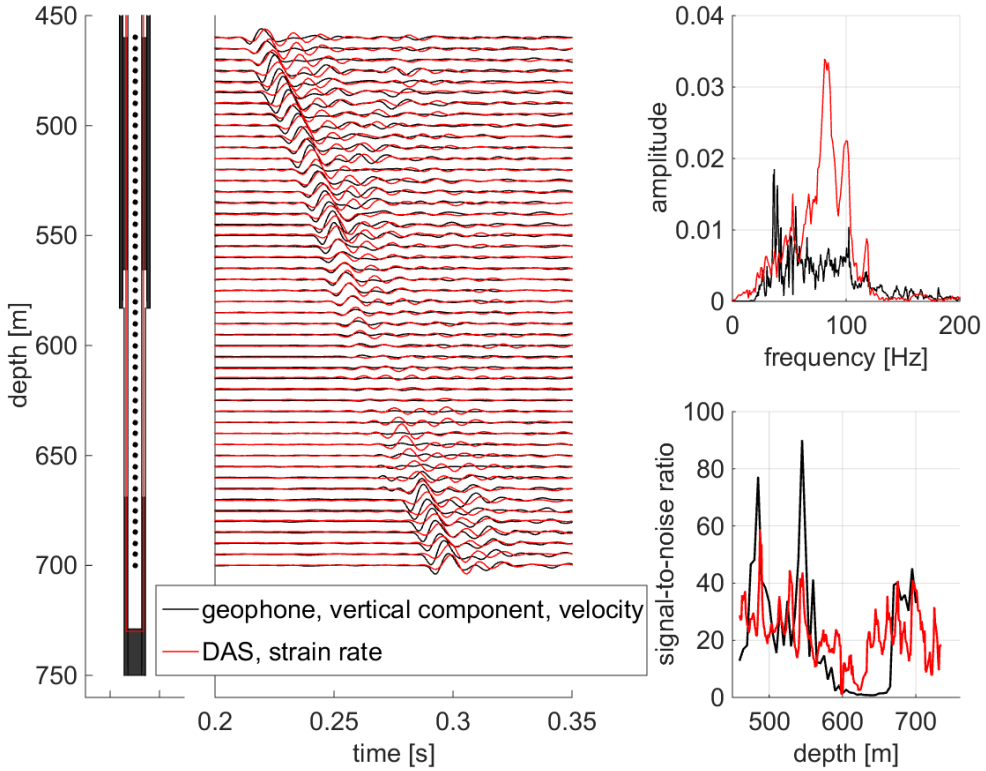

Figure 20: Comparison between the vertical component of borehole geophones (velocity, VIBSIST source) and the DAS recordings (strain rate, Vibroseis source). Left: Well completion of well Ktzi202 with the locations of 3C geophones (black dots) and the fibre-optical cable (red line). The optical fibre is installed behind the production casing. Cemented intervals are indicated by grey sections in the well diagram. Middle: Wiggle plot of the seismic traces. Right: Comparison of amplitude spectrum and signal-to-noise ratios for the depth interval 450 m – 700 m. Modified after Reinsch *et al.* 2015.

The downgoing wavelets for both recording methods differ due to the different source types (VIBSIST vs. Vibroseis) and pre-processing methods (shift-and-stack vs correlation). This is e.g. reflected in the frequency spectra of the measurements. Due to the employed sweep from 7 – 120 Hz, the frequency content of the DAS measurement is higher than that of the geophone recordings (Figure 9, top right). Moreover the different physical quantities measured have to be taken into account. Daley *et al.* (2016) have shown that DAS data can be converted to a geophone-equivalent signal. For the native strain-rate data, a phase shift of 90° to velocity should be present. Nevertheless, some comparative observations can be made. The influence of the cementation of the casing on both data sets is similar. Clear first breaks can be observed only for fully cemented casing sections, e.g. 460 m – 565 m and 670 m – 700 m. The signal fades between 565 m and 670 m depth, where the production casing is not cemented to the formation (this is the reservoir level). Between 605 m and 625 m depth it is not possible to identify any first breaks. At 630 m the first breaks of the DAS traces start to recover, contrary to the geophone traces.

Experience has shown that also for uncemented casing strings, which have been in place for sufficient time, a reasonable mechanical coupling or bond between casing and formation is often developed, e.g. Hardage 2000. This is the result from successively filling the annulus with solid material, e.g. settling of concretions or cuttings from the drilling mud, or sloughing of the formation, over time. For the Ktzi202 well, such a process has been inferred to occur from analysis of time-lapse pulsed neutron-gamma logs for an interval with increasing extent from 642 – 636 m depth over successive years between 2008 and 2012 (Baumann, Henninges and De Lucia 2014). Moreover, the brine level increased from 651 m during the geophone VSP recording in 2011 to 634 m before the DAS-VSP survey, both inside the casing and the well annulus (Baumann, Henninges and De Lucia 2014). Therefore the higher DAS-VSP signal-to-noise ratio is attributed to a combination of these effects within the lower part of the affected zone.

A similar effect can be observed when comparing the signal-to-noise ratio (Figure 9, bottom right). With the DAS technique, the signal-to-noise ratio of conventional geophone recordings can be reached. It should be noted that the good signal-to-noise-ratio of the DAS data was achieved due to a rather powerful source, to the amount of stacking and the long sweeps (Chapter 2). In the depth interval of the uncemented production casing, the DAS data maintain a higher signal-to-noise ratio than the geophone data, probably due to the deployment behind casing. Better comparability between the recordings could have been reached by wavelet matching.

7 DAS-VSP cube

The 3D surface seismic cube is converted from time domain to depth domain by using stacking velocities derived for the baseline data (Juhlin *et al.* 2007). The depth conversion is tied to sonic logs, especially using the strong reflection of the anhydrite layer (Top Weser Formation, Figure 1, Figure 10). In Figure 10 the bandpass filtered (10-20-80-100 Hz) DAS-VSP cube is compared to the 3D surface seismic data.

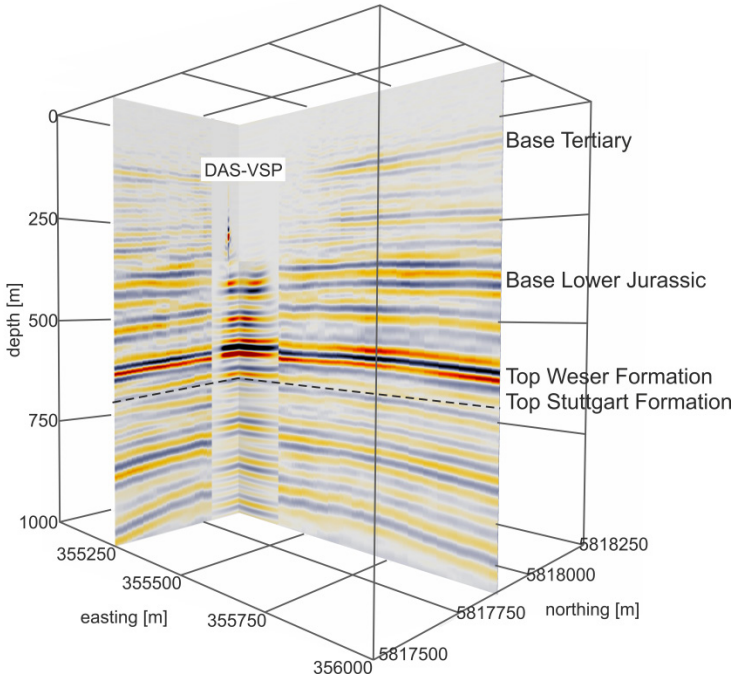

Figure 21: Comparison of bandpass filtered DAS-VSP cube (10-20-80-100 Hz) and the depth converted 3D surface seismic cube (Ivandic *et al.* 2015). For reasons of good visibility, the DAS-VSP slices are shown 12 m in front of the 3D surface seismic cube.

The 3D depth migration of the DAS-VSP data was performed with a relatively simple velocity model based on sonic logs (Chapter 3). With this velocity model a good tie between the DAS-VSP cube and the existing surface seismic data was achieved at the Top of the Stuttgart Formation. Especially below the Stuttgart Formation, where no sonic log velocities and structural information was available a substantial mismatch between both cubes can be observed. As stated in Chapter 3 the tie could be improved by using a heterogeneous velocity model, taking into account the variation of velocities within the layers. It is possible to image the subsurface down to at least 1000 m, which is the same depth as for the 3D surface seismic (Juhlin *et al.* 2007).

Based on well cores, the depth of the top of the Stuttgart Formation is determined by the transition of the Weser Formation (mudstones) to the Stuttgart Formation (siltstones-sandstones, Förster *et al.* 2010). The distance between the top of the Weser Formation (K2 reflector) and the top of the Stuttgart Formation (the reservoir), is about 70 m. The reservoir is located at the top of the Stuttgart Formation in 630 – 650 m depth and consists of sandstones (channel facies rocks) and mudstones (flood-plain facies rocks, Norden and Frykman 2013). The transition from the Weser Formation to the

Stuttgart Formation is rather smooth, from higher to lower impedances, characterised by only a weak, negative reflection signal in the seismic data.

Through the injected CO_2, the impedance contrast between the Weser Formation and the reservoir is increased and the reservoir becomes visible in the seismic data, but is still not easy to pick in the 3D surface seismics (Figure 11, left).

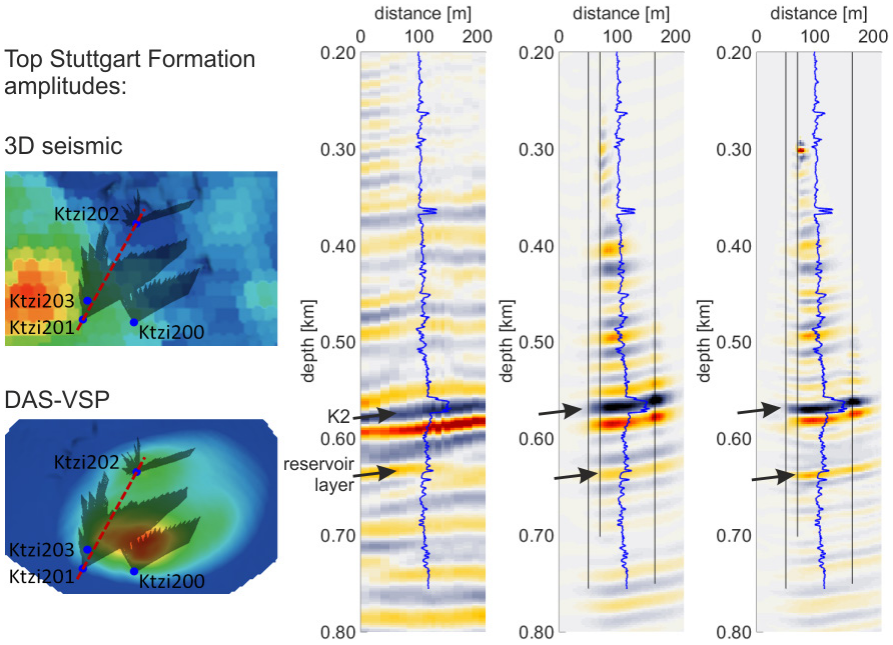

Figure 22: Comparison of 3D surface seismic, bandpass filtered DAS-VSP and raw DAS-VSP. Left: Top view on the seismic amplitudes extracted from the top of the Stuttgart Formation for the 3D seismic and DAS-VSP. The black shaded areas indicate the DAS-VSP reflection loci. Red line shows location of sections (right). Right: Cross sections extracted between the wells Ktzi201 and Ktzi202. The wells Ktzi201, Ktzi203 and Ktzi202 are indicated by the black lines and the impedance log for the well Ktzi201 is inserted (blue line).

The reflections from the reservoir can be clearly identified in the DAS-VSP data, firstly because of the smaller distance between the VSP channels and the reservoir and secondly because of the higher frequency content of the data. More details of the structure above the K2 reflector as well as below the reservoir are shown in the DAS-VSP data.

The coverage of the VSP data is limited (Figure 11, left) due to the limited offset between the source points and the receiver wells. For instance, the distance between Ktzi201 and Ktzi202 (about 100 m) is not entirely covered, leading to higher amplitudes at the wells and a fading of the amplitudes in between the wells. This can be observed e.g. at the reflections from the anhydrite layer (Figure 11, right) or at the amplitudes extracted at the Top of the Stuttgart Formation (Figure 11, left).

8 Conclusion

The field tests at the Ketzin CO_2 storage site demonstrated that DAS can be used for recording simultaneous multi-well VSP data with a single interrogator unit. As long as the coupling with the formation is present, good signal-to-noise ratios are obtained for all of the source points, downgoing and upgoing waves are observed within every well. It was possible to record simultaneously within four wells, covering the whole length of the wells with a single shot in a very fine depth sampling. It has been shown that DAS-VSP data with complex acquisition geometry can be acquired fast and cost-efficiently. Furthermore, the optical-fibre VSP technique is a permanent acquisition system, and can be used in different periods of the well's life, thus enabling time-lapse VSP analysis for monitoring. Thus, on-demand and time-lapse VSP measurements become operationally feasible with reduced logistical effort compared to conventional wireline acquisition. Permanently deployed fibre optic cables enable time-lapse VSP surveys using pressurized wells, where conventional seismic surveys using wireline equipment are possible only under highly restricted conditions (pressure equipment, short receiver arrays). Extended stacking of sweeps resulted in VSP shot gathers with a signal-to-noise ratio comparable to gathers acquired using conventional geophone deployment. It was possible to build a focused, high resolution depth migrated DAS-VSP cube, to image the structure right below the injection site, though with limited lateral resolution caused by the acquisition geometry. This could be overcome by extending the source point distribution to larger offsets from the wells and by optimized source point locations around the well locations.

Acknowledgements

The authors gratefully acknowledge the funding for the Ketzin project received from the European Commission (6^{th} and 7^{th} Framework Program), two German ministries - the Federal Ministry of Economics and Technology and the Federal Ministry of Education and Research - and industry since 2004. The ongoing R&D activities are funded within the project COMPLETE by the Federal Ministry of Education and Research. Further funding is received by VGS, RWE, Vattenfall, Statoil, OMV and the Norwegian CLIMIT programme. We also acknowledge Ms. Mary Humphries, Director, VSProwess Ltd, UK, who provided the VSProwess software and helped to set up the processing and imaging routines. Two anonymous reviewers provided very constructive comments which helped to improve the paper significantly.

References

Barberan, C., Allanic, C., Avila, D., Hy-Billiot, J., Hartog, A., Frignet, B. and Lees, G. (2012). Multi-offset Seismic Acquisition Using Optical Fiber Behind Tubing. 74th EAGE Conference & Exhibition incorporating SPE EUROPEC 2012, Copenhagen, Denmark, extended abstract Y003.

685 Baumann, G., Henninges, J. and De Lucia, M. (2014). Monitoring of saturation changes and salt
686 precipitation during CO_2 injection using pulsed neutron-gamma logging at the Ketzin site. Intl J
687 Greenhouse Gas Control 28, 134-146.

688 Bergmann, P., Ivandic, M., Norden, B., Rücker, C., Kiessling, D., Lüth, S., Schmidt-Hattenberger, C. and
689 Juhlin, C. (2014). Case History: Combination of seismic reflection and constrained resistivity inversion
690 with an application to 4D imaging of the CO_2 storage site, Ketzin, Germany. Geophysics 79(2), B37–
691 B50.

692 Chadwick, A., Williams, G., Delepine, N., Clochard, V., Labat, K., Sturton, S., Buddensiek, M.-L., Dillen,
693 M., Nickel, M., Lima, A. L., Arts, R., Neele, F. and Rossi, G. (2010). Quantitative analysis of time-lapse
694 seismic monitoring data at the Sleipner CO_2 storage operation. The Leading Edge 29(2), 170–177.

695 Cosma, C. and Enescu, N. (2001). Characterization of fractured rock in the vicinity of tunnels by the
696 swept impact seismic technique. International Journal of Rock Mechanics & Mining Sciences 38, 815–
697 821.

698 Daley, T., Freifeld, B., Ajo-Franklin, J., Dou, S., Pevzner, R., Shulakova, V., Kashikar, S., Miller, D., Götz,
699 J., Henninges, J. and Lüth, S. (2013). Field testing of fiber-optic distributed acoustic sensing (DAS) for
700 subsurface seismic monitoring. The Leading Edge 32, 699–706.

701 Daley, T.M., Miller, D.E., Dodds, K., Cook, P. & Freifeld, B.M. 2016. Field testing of modular borehole
702 monitoring with simultaneous distributed acoustic sensing and geophone vertical seismic profiles at
703 Citronelle, Alabama. Geophysical Prospecting 64, 1318–1334.

704 Dean, T., Cuny, T. & Hartog, A.H. 2017. The effect of gauge length on axially incident P-waves
705 measured using fibre optic distributed vibration sensing. Geophysical Prospecting 65, 184–193.

706 Dillon, P.B. and Thomson, R.C. (1984). Offset source VSP surveys and their image reconstruction.
707 Geophysical Prospecting 32, 790–811.

708 Egreteau, A., Gibson, J., Lin F. and Meunier, J. (2009). Using long sweep in land vibroseis acquisition.
709 71st EAGE Conference & Exhibition, Amsterdam, The Netherlands, extended abstract.

710 Förster A., Norden B., Zinck-Jørgensen K., Frykman P., Kulenkampff J., Spangenberg E., Erzinger J.,
711 Zimmer M., Kopp J., Borm G., Juhlin C., Cosma C. and Hurter S. (2006). Baseline characterization of
712 the CO_2SINK geological storage site at Ketzin, Germany. Environmental Geosciences 13(3), 145–161.

Förster, A., Schöner, R., Förster, H.-J., Norden, B., Blaschke, A.-W., Luckert, J., Beutler, G., Gaupp, R. and Rhede, D. (2010). Reservoir characterization of a CO_2 storage aquifer: The Upper Triassic Stuttgart Formation in the Northeast German Basin. Marine and Petroleum Geology 27, 2156–2172.

Frignet, B. and Hartog, A. (2014). Optical Vertical Seismic Profile On Wireline Cable. SPWLA 55th Annual Logging Symposium, Abu Dhabi, May 18-22, extended abstract.

Giese, R., Henninges, J., Lüth, S., Morozova, D., Schmidt-Hattenberger, C., Würdemann, H., Zimmer, M., Cosma, C. and Juhlin, C. (2009). Monitoring at the CO_2SINK site: A concept integrating geophysics, geochemistry and microbiology. Energy Procedia, 1(1), 2251–2259.

Götz, J. (2014). Borehole seismic monitoring of CO_2 storage within a saline aquifer at Ketzin, Germany. PhD Thesis, TU Berlin, Germany, 125 p.

Götz, J., Lüth, S., Krawczyk, C.M., and Cosma, C. (2014). Zero-Offset VSP Monitoring of CO_2 Storage: Impedance Inversion and Wedge Modelling at the Ketzin Pilot Site. International Journal of Geophysics, 2014, Article ID 294717, 15 pages.

Götz, J., Lüth, S., Henninges, J. and Reinsch T. (2015). Using a fibre optic cable as Distributed Acoustic Sensor for Vertical Seismic Profiling at the Ketzin CO_2 storage site. - 77th EAGE Conference & Exhibition, Madrid, Spain, extended abstract Th P2 13.

Hansen, O., Eiken, O., Ostmo, S., Johansen, R.I., and Smith, A. (2011). Monitoring CO_2 injection into a fluvial brine-filled sandstone formation at the Snøhvit field, Barents Sea. SEG San Antonio 2011 Annual Meeting, extended abstract SEG-2011-4092.

Hardage, B.A. 2000. Vertical seismic profiling: principles; Third updated and revised edition. Pergamon, ISBN 0-08-043518-1.

Hartog, A., Kotov, O., and Liokumovich, L. (2013). The Optics of Distributed Vibration Sensing. - Second EAGE Workshop on Permanent Reservoir Monitoring 2013 - Current and Future Trends Stavanger, Norway, extended abstract Th_01_04.

Hartog, A., Frignet, B., Mackie, D. and Clark, M. (2014). Vertical seismic optical profiling on wireline logging cable. Geophysical Prospecting, 62(4), 693–701.

Henninges, J., Liebscher, A., Bannach, A., Brandt, W., Hurter, S., Köhler, S., Möller, F. and CO_2SINK-Group (2011). P-T-ρ and two-phase fluid conditions with inverted density profile in observation wells at the CO_2 storage site at Ketzin (Germany). Energy Procedia 4, 6085–6090.

742 Hill, D. (2013). Distributed Acoustic Sensing for Permanent Downhole Monitoring. Second EAGE
743 Workshop on Permanent Reservoir Monitoring 2013 - Current and Future Trends Stavanger, Norway,
744 extended abstract Th_01_05.

745 Hovorka, S.D., Benson, S.M., Doughty, C., Freifeld, B.M., Sakurai, S., Daley, T.M., Kharaka, Y.K., Holtz,
746 M.H., Trautz, R.C., Nance, H.S., Myer, L.R. and Knauss, K.G. (2006). Measuring permanence of CO_2
747 storage in saline formations: the Frio experiment. Environmental Geosciences 13(2), 105–121.

748 Hovorka, S.D., Meckel, T.A. and Treviño, R. H. (2013). Monitoring a large-volume injection at
749 Cranfield, Mississippi-Project design and recommendations. International Journal of Greenhouse Gas
750 Control 18, 345–360.

751 Huang, F., Juhlin, C., Kempka, T., Norden, B. and Zhang, F. (2015). Modeling 3D time-lapse seismic
752 response induced by CO_2 by integrating borehole and 3D seismic data - A case study at the Ketzin
753 pilot site, Germany. International Journal of Greenhouse Gas Control 36, 66–77.

754 Humphries, M., Vidal, J.A.M. and de Dios, J.C. (2015. VSP Monitoring for CO_2 Migration Tracking in
755 Fractured Rock Massifs. 77th EAGE Conference & Exhibition, Madrid, Spain, extended abstract Tu
756 N112 02.

757 IPCC (2005). Special Report on Carbon Dioxide Capture and Storage. Prepared by Working Group III of
758 the Intergovernmental Panel on Climate Change, Cambridge University Press, New York, NY, USA.

759 Ivandic, M., Yang, C., Lüth, S., Cosma, C. and Juhlin, C. (2012). Time-lapse analysis of sparse 3D
760 seismic data from the CO_2 storage pilot site at Ketzin, Germany. Journal of Applied Geophysics 84,
761 14–28.

762 Ivandic, M., Juhlin, C., Lüth, S., Bergmann, P., Kashubin, A., Sopher, D., Ivanova, A., Baumann, G. and
763 Henninges, J. (2015). Geophysical monitoring at the Ketzin pilot site for CO_2 storage: New insights
764 into the plume evolution. International Journal of Greenhouse Gas Control 32, 90–105.

765 Ivanova, A., Kashubin, A., Juhojuntti, N., Kummerow, J., Henninges, J., Juhlin, C., Lüth, S. and Ivandic,
766 M. (2012). Monitoring and volumetric estimation of injected CO_2 using 4D seismic, petrophysical
767 data, core measurements and well logging: a case study at Ketzin, Germany. Geophysical
768 Prospecting, 60(5), 957–973.

769 Juhlin, C., Giese, R., Zinck-Jørgensen, K., Cosma, C., Kazemeini, H., Juhojuntti, N., Lüth, S., Norden, B.
770 and Förster, A. (2007). Case History: 3D baseline seismics at Ketzin, Germany: The CO_2SINK project.
771 Geophysics, 72(5), B121–B132.

772 Kikuta, K., Hongo, S., Tanase, D. and Ohsumi, T. (2005). Field test of CO_2 injection in Nagaoka, Japan.
773 In Proc. 7th Int. Conf. on Greenhouse Gas Control Technologies, vol. 2 (eds E.S. Rubin, D.W. Keith and
774 C.F. Gilboy), 1367–1372. Oxford, UK: Elsevier.

775 Kuvshinov, B. N. (2015). Interaction of helically wound fibre-optic cables with plane seismic waves.
776 Geophysical Prospecting, 64(3), 671-688.

777 Lüth, S., Ivanova, A., Ivandic, M. and Götz, J. (2015). 4D seismic monitoring at the Ketzin pilot site
778 during five years of storage – results and quantitative assessment. Energy Procedia 76, 536–542.

779 Madsen, K., Thompson, M., Parker, T. and Finfer, D. (2013). A VSP field trial using distributed acoustic
780 sensing in a producing well in the North Sea. First break 31, 51–56.

781 Martens, S., Liebscher, A., Möller, F., Henninges, J., Kempka, T., Lüth, S., Norden, B., Prevedel, B.,
782 Szizybalski, A., Zimmer, M., Kühn, M. and the Ketzin Group (2013). CO_2 storage at the Ketzin pilot
783 site, Germany: Fourth year of injection, monitoring, modelling and verification. Energy Procedia 37,
784 6434–6443.

785 Martens, S., Möller, F., Streibel, M., Liebscher A. and The Ketzin Group (2014). Completion of five
786 years of safe CO_2 injection and transition to the post-closure phase at the Ketzin pilot site. Energy
787 Procedia 59, 190–197.

788 Martens, S., Conze, R., De Lucia, M., Henninges, J., Kempka, T., Liebscher, A., Lüth, L., Möller, F.,
789 Norden, B., Prevedel, B., Schmidt-Hattenberger, C., Szizybalski, Vieth-Hillebrand, A., Würdemann, H.,
790 Zemke, K. and Zimmer, M. (2015). Joint Research Project CO_2MAN (CO_2MAN Reservoir
791 Management): Continuation of Research and Development Work for CO_2 Storage at the Ketzin Pilot
792 Site. In: A. Liebscher and U. Münch (eds.), Geological Storage of CO_2 – Long Term Security Aspects,
793 Advanced Technologies in Earth Sciences, Springer International Publishing Switzerland, 1–32.

794 Mateeva, A., Lopez, J., Potters, H., Mestayer, J., Cox, B., Kiyashchenko, D., Wills, P., Grandi, S.,
795 Hornman, K., Kuvshinov, B., Berlang, W., Yang, Z. and Detomo, R. (2014). Distributed acoustic sensing
796 for reservoir monitoring with vertical seismic profiling. Geophysical Prospecting 62, 679–692.

797 Mateeva, A. and Zwartjes, P.M. (2017). Depth Calibration of DAS VSP Channels - A New Data-Driven
798 Method. 79th EAGE Conference and Exhibition, extended abstract, DOI: 10.3997/2214-
799 4609.201701201.

800 Mestayer, J., Cox, B., Wills, P., Kiyashchenko, D., Lopez, J., Costello, M., Bourne, S., Ugueto, G.,
801 Lupton, R., Solano, G., Hill, D. and Lewis, A. (2011). Field Trials of Distributed Acoustic Sensing for
802 Geophysical Monitoring. SEG Annual Meeting San Antonio, extended abstract.

803 Mewhort, L., Bezdan, S. and Jones, M. (2002). Does it Matter What Kind of Vibroseis Deconvolution is
804 Used? CSEG Geophysics, extended abstract, 1-4.

805 Molenaar, M., Hill, D., Webster, P., Fidan, E. and Birch, B. (2011). First Downhole Application of
806 Distributed Acoustic Sensing (DAS) for Hydraulic Fracturing Monitoring and Diagnostics. SPE
807 Hydraulic Fracturing Technology Conference, The Woodlands, Texas, extended abstract SPE 140561.

808 Norden, B. and Frykman, P. (2013). Geological modelling of the Triassic Stuttgart Formation at the
809 Ketzin CO_2 storage site, Germany. International Journal of Greenhouse Gas Control 19, 756–774.

810 Parker, T., Shatalin, S. and Farhadiroushan, M. (2014). Distributed Acoustic Sensing - a new tool for
811 seismic applications. First Break 32, 61–69.

812 Prevedel, B., Wohlgemuth, L., Legarth, B., Henninges, J., Schütt, H., Schmidt-Hattenberger, C.,
813 Norden, B., Förster, A. and Hurter, S. (2009). The CO_2SINK boreholes for geological CO_2-storage
814 testing. Energy Procedia 1, 2087–2094.

815 Prevedel, B., Martens, S., Norden, B., Henninges, J. and Freifeld, B.M. (2014). Drilling and
816 abandonment preparation of CO_2 storage wells – Experience from the Ketzin pilot site. Energy
817 Procedia 63, 6067–6078.

818 Reinsch, T., Henninges, J., Götz, J., Jousset, P., Bruhn, D. and Lüth, S. (2015). Distributed Acoustic
819 Sensing Technology for Seismic Exploration in Magmatic Geothermal Areas. Proceedings World
820 Geothermal Congress 2015, Melbourne, Australia, extended abstract.

821 Ringrose, P.S., Mathieson, A.S., Wright, I.W., Selama, F., Hansen, O., Bissell, R., Saoula, N. and
822 Midgley, J. (2013). The in Salah CO_2 storage project: lessons learned and knowledge transfer. Energy
823 Procedia 37, 6226–6236.

824 Schmidt-Hattenberger, C., Bergmann, P., Labitzke, T. and Wagner, F. (2014). CO_2 migration
825 monitoring by means of Electrical Resistivity Tomography (ERT) - Review on five years of operation of
826 a permanent ERT system at the Ketzin pilot site. Energy Procedia 6, 4366–4373.

827 Staples, R.K., Hobbs, R.W. and White, R.S. (1999). A comparison between airguns and explosives as
828 wide-angle seismic sources. Geophysical Prospecting 47, 313–339.

829 Underschultz, J., Boreham, C., Dance T., Stalker, L., Freifeld, B., Kirste, D. and Ennis-King, J. (2011).
830 CO_2 storage in a depleted gas field: an overview of the CO2CRC Otway Project and initial results.
831 International Journal of Greenhouse Gas Control 5(4), 922–932.

832 Whittaker, S., Rostron, B., Hawkes C., Gardner, C., White, D., Johnson, J., Chalaturnyk, R. and
833 Seeburger, D. (2011). A decade of CO2 injection into depleting oil fields: monitoring and research
834 activities of the IEA GHG Weyburn-Midale CO_2 monitoring and storage project. Energy Procedia 4,
835 6069–6076.

836 Yang, C., Juhlin, C., Enescu, N., Cosma, C., and Lüth, S. (2010). Moving source profile data processing,
837 modelling and comparison with 3D surface seismic data at the CO_2SINK project site, Ketzin, Germany.
838 Near Surface Geophysics 8, 601–610.

839 Yordkayhun, S., Ivanova, A., Giese, R., Juhlin, C. and Cosma, C. (2009). Comparison of surface seismic
840 sources at the CO_2SINK site, Ketzin, Germany. Geophysical Prospecting 57, 125–139.

841 Zhang, F., Juhlin, C., Cosma, C., Tryggvason, A. and Pratt, R. (2012). Cross-well seismic waveform
842 tomography for monitoring CO_2 injection: a case study from the Ketzin Site, Germany. Geophysical
843 Journal International 189(1), 629–646.